

Two Compton-Thick Active Nuclei in Arp 220?

Alessandro Paggi¹, Giuseppina Fabbiano¹, Guido Risaliti^{1,2}, Junfeng Wang¹ and Martin Elvis¹

¹*Harvard-Smithsonian Center for Astrophysics, 60 Garden St, Cambridge, MA 02138, USA:*

apaggi@cfa.harvard.edu

²*INAF-Arcetri Observatory, Largo E. Fermi 5, I-50125 Firenze, Italy*

ABSTRACT

Narrow-band spectral imaging with sub-pixel resolution of the *Chandra*-ACIS archival observation of the ULIRG merger Arp 220 strongly suggests two Compton thick nuclei, spatially coincident with the infrared and radio emitting nuclear clusters, and separated by 1'' (~ 365 pc at a distance of 76 Mpc). These previously undetected highly obscured AGNs - West (W) and East (E) - are imaged, and separated from neighboring sources, in the 6-7 keV band, where the Fe-K lines dominate the emission. The western nucleus is also detected at energies above 7 keV. We estimate Fe-K equivalent width ~ 1 keV or possibly greater for both sources, and observed 2-10 keV luminosities $L_X < 3.2 \times 10^{40}$ erg s⁻¹ (W) and $< 1.3 \times 10^{40}$ erg s⁻¹ (E). From the observed Fe-K lines luminosities, and assuming on the basis of the *XMM-Newton* spectrum that 40% of this may be from the 6.4 keV component, we evaluate 2-10 keV intrinsic luminosities $L_X \sim 1 \times 10^{42}$ erg s⁻¹ (W) and $L_X \sim 0.4 \times 10^{42}$ erg s⁻¹ (E). The inferred X-ray luminosity is at least a factor of 3 higher than that expected from a pure starburst with the bolometric luminosity of Arp 220. For a typical AGN SED the bolometric luminosities are 5.2×10^{43} erg s⁻¹ (W) and 2×10^{42} erg s⁻¹ (E).

Subject headings: galaxies: active — galaxies: individual (Arp 220) — galaxies: Seyfert — galaxies: interactions — X-rays: galaxies

1. INTRODUCTION

The M- σ relation (e.g., [Magorrian et al. 1998](#)) has suggested that the evolution of galaxies and super-massive nuclear black holes (SMBHs) are linked. Both the stellar population and the SMBH of a galaxy are thought to grow and evolve by merging of smaller gas-rich galaxies and their nuclear SMBHs ([Di Matteo, Springel, & Hernquist 2005](#); [Hopkins, McClure-Griffiths, & Gaensler](#)

2008). During this process, the SMBH may be “buried” by thick molecular gas, which feeds the SMBH at high rates, causing the birth of an obscured Compton Thick (CT, [Risaliti, Maiolino, & Salvati 1999](#); [Levenson et al. 2006](#)) Active Galactic Nucleus (AGN). CT AGNs are characterized in the X rays by a hard high energy continuum, a “reflection” flat continuum in the $\sim 2 - 10$ keV range, and a very high Equivalent Width (EW) $\gtrsim 1$ keV 6.4 Fe-K α line (e.g., [Matt et al. 1997, 2000](#)). Examples of this merger-driven evolution are given by the pairs of nuclei discovered in the 6.4 keV Fe-K line with *Chandra* in the merger infrared (IR) luminous galaxy NGC 6240 ([Komossa et al. 2003](#)) and in the CT AGN NGC 3393 ([Fabbiano et al. 2011](#)).

At a distance of 76 Mpc ([Kim & Sanders 1998](#)), Arp 220 (IC 4553/4) is both a merger, and the nearest Ultra-luminous IR Galaxy (ULIRG; [Soifer et al. 1987](#); [Sanders & Mirabel 1996](#)). Near IR high-resolution (0.1”) NICMOS-HST imaging identifies the two nuclear regions of the merging galaxies, which are coincident with the two components of a double radio source ([Baan & Haschick 1995](#); [Scoville et al. 1998](#)). At a separation of 0.98” (361 pc at a distance of 76 Mpc¹), these nuclei are closer together than the nuclei of NGC 6240 (~ 690 pc separation, [Komossa et al. 2003](#)), and therefore should be subject to even stronger gravitational interaction and possible accretion. Indeed, the presence of an AGN with a contribution to the bolometric luminosity between ~ 5 and $\sim 25\%$, and a best estimate of 18%, is suggested by the Spitzer Mid-IR spectrum of the central 8” region of Arp 220 ([Veilleux et al. 2009](#); [Nardini et al. 2010](#); more recent *Herschel* results ([Rangwala et al. 2011](#)) and modeling of the nuclear spectra ([Contini 2012](#)) agree with this conclusion. The presence of a maser ([Aalto et al. 2009](#)) and a rotating massive molecular disk ([Downes & Eckart 2007](#)) suggests a massive nuclear black hole in the west nucleus of Arp 220.

A high resolution study with a ~ 57 ks *Chandra* ACIS observation (obsid 869; [Clements et al. 2002](#)) failed to secure the firm identification of nuclear AGN emission, reporting the presence of three hard X-ray sources in the region, of which two (X-1 and X-4, see their Figure 2) are near, but not coincident with, the nuclear radio sources. The X-ray spectrum extracted from the central ~ 2 ” region showed complexity, with a possible hard component and Fe-K line. Subsequent *XMM-Newton* observation detected Fe-K line emission centered at 6.7 keV with EW ~ 1.9 keV ([Iwasawa et al. 2005](#)) suggesting highly photoionized, low-density gas illuminated by a hidden CT AGN. A re- analysis of the *Chandra* data ([LaMassa et al. 2011](#)) only manages to set an upper limit on the Fe-K α EW assuming a 6.4 keV line energy. The nature of the X-ray emission of Arp 220 is therefore still elusive.

In this paper we re-examine the question of the X-ray AGN emission of Arp 220, by means of sub-pixel imaging of *Chandra* ACIS data in narrow spectral ranges. This technique has been

¹In the following, we adopt the standard flat cosmology with $\Omega_A = 0.73$ and $H_0 = 70 \text{ km s}^{-1} \text{ Mpc}^{-1}$ ([Komatsu et al. 2011](#)).

used successfully to study crowded emission regions of nearby Seyferts (e.g. in NGC 4151 [Wang et al. 2011a,b,c](#); Mrk 573, [Paggi et al. 2012](#)); in the nearby CT AGN NGC 3393, it has led to the discovery of two CT nuclei, with 150 pc separation ([Fabbiano et al. 2011](#)). Our new look at the nuclear region of Arp 220, has resulted in the discovery of two sources in the 6-7 keV Fe-K band, strongly suggestive of CT nuclei. These sources are spatially coincident with the near-IR and radio positions. Below we discuss our technique and results.

2. Data Analysis

Arp 220 was observed by *Chandra* on 2000 June 24 for 57 ks (Obs. ID 869, PI: Clements). Level 2 event data were retrieved from the *Chandra* Data Archive² and reduced with the CIAO ([Fruscione et al. 2006](#)) 4.4 software and the *Chandra* Calibration Data Base (CALDB) 4.5.3, adopting standard procedures. After excluding time intervals of background flares exceeding 3σ with the LC_SIGMA_CLIP task, we obtained a low-background exposure time of ~ 56 ks. The nucleus has no significant pile up, as measured by the CIAO PILEUP_MAP tool. Imaging analysis was performed without pixel randomization to take advantage of the telescope dithering in event positioning and with the sub-pixel event repositioning (SER) procedure ([Li et al. 2003](#)). We used a pixel size $1/4$ of $0.492''$, the native *Chandra*/ACIS detector pixel (see, e.g., [Harris et al. 2004](#); [Siemiginowska et al. 2007](#); [Perlman et al. 2010](#); [Wang et al. 2011a](#)).

Using the same Orion ACIS-S data as in the calibration of [Li et al. \(2003\)](#), we find a significant $\Delta = 50\%$ (improvement in PSF FWHM as defined in [Li et al. 2003](#)) from sub-pixel repositioning for an on-axis source at 6-7 keV ($\Delta = 70\%$ at ~ 2 keV because of the narrower PSF). Most of the imaging improvement is from sub-pixel binning, which uses the sampling of the PSF by the well characterized spacecraft dither motion. Because of the similarly ‘peaked’ inner PSF this is similarly effective at 2 and 6 keV.

The resulting full band (0.5-10 keV) ACIS image is presented in the left panel of Figure 1. This figure shows complexity in the central region of Arp 220, but there is no X-ray feature that can be univocally associated with the radio/IR nuclei. Instead, narrow band imaging (6-7 keV containing the Fe-K lines) reveals these hidden nuclei (Figure 1, right panel). The only sources of emission in this spectral band are localized in two regions separated by $\sim 1''$ (corresponding to ~ 365 pc at a distance of 76 Mpc) and co-located with the NIR $2.2\mu\text{m}$ ([Scoville et al. 1998](#)) and radio nuclei ([Baan & Haschick 1995](#)). Following [Scoville et al. 1998](#), we have shifted the VLA 6 cm sources in the NE direction by $\sim 0.13''$ in order to match the position of the western lobe with

²<http://cda.harvard.edu/chaser>

the western nucleus. We note that the eastern radio lobe results somewhat dislocated from eastern narrow-band nucleus. However, due to the low counts in this region, the location of this emission is consistent within uncertainties with the radio lobe. Under this assumptions, radio, NIR and Fe-K nuclei are consistent within astrometric uncertainties. Deeper *Chandra* X-ray observations are needed for convincingly evaluate if the position of the E nucleus is in better agreement with the IR or radio position. We note that the extension of the narrow-band emission in the east direction is not due to PSF asymmetries, as indicated by the `MAKE_PSF_ASYMMETRY_REGION` tool that shows PSF artifacts in the north-west direction.

We extracted counts from the $0''.5$ circles centered at RA=15:34:57.252 DEC=+23:30:11.64 (W) and RA=15:34:57.326 DEC=+23:30:11.84 (E) (Figure 2, upper panel); *Chandra* absolute astrometric uncertainty is $0''.6$. We find in the 6-7 keV band 12 counts associated with the Western nucleus (W), and 3 counts associated with the Eastern nucleus (E). Note that the background emission in this band is 0.01 counts in the same area of the extraction regions, so even a 3 counts detection is a highly significant source ($P < 10^{-6}$ of chance detection, corresponding to a $\sim 5\sigma$ Gaussian significance).

Given the energy dependent grade branching ratio for BI ACIS CCD (Li et al. 2003), and since sub-pixel repositioning is more uncertain for 1 pixel (GRADE=0) events than for 2 pixel (GRADE=2,3,4) and 4 pixel (GRADE=6) events, we checked the event grade distribution in W and E regions to ensure reliability of events position with SER. The majority of W region events are 2 and 4 pixel, while no 1 pixel event is found in E region. Therefore sub-pixel analysis improves the positioning of these events.

The flux in this band, however, is highly uncertain due to the low counts. In this case, approximate narrow-band model-independent fluxes can be estimated with the CIAO `APRATES` tool, to yield $0.7^{+0.5}_{-0.4} \times 10^{-14}$ erg cm $^{-2}$ s $^{-1}$ (E) and $1.9^{+0.8}_{-0.6} \times 10^{-14}$ erg cm $^{-2}$ s $^{-1}$ (W). These correspond to 6-7 keV observed luminosities $5.2^{+3.7}_{-2.5} \times 10^{39}$ erg s $^{-1}$ (E) and $13.8^{+5.9}_{-4.7} \times 10^{39}$ erg s $^{-1}$ (W).

The locations of these unique emission regions strongly argue for an identification of these sources with the nuclei of the merging galaxies. Although the W source is positionally coincident with the X-4 hard X-ray source reported by Clements et al. (2002) (see Figure 1), the sub-pixel narrow band imaging suggests a different picture. Figure 2 (middle panel) shows the 3-6 keV band image, where the most prominent source is found to the west of both W and of the reported X-4 position (Clements et al. 2002). Figure 2 (lower panel) shows the emission in the 7-10 keV band, suggesting hard continuum emission from the W nucleus (3 cts) with $P \sim 10^{-5}$ of chance detection. The CIAO `APRATES` tool gives in this region 7^{+5}_{-3} cts, while we derive a firm 2 counts upper limit in the E nucleus region. These images suggest the presence of highly obscured CT AGN in the nuclei.

The narrow-band images (Figure 2) also show that the continuum emission from the nuclei

is contaminated by unrelated sources even at *Chandra* resolution. Nevertheless, we attempted a spectral characterization of the emission, extracting 3-8 keV spectra from the two circular regions (0.5'' radius) indicated in Figure 2 with the CIAO `SPEXTRACT` task, applying point-source aperture correction. We then fitted simultaneously the two spectra employing the Cash statistic. We used a model typical of CT AGN emission (Levenson et al. 2006), comprising an absorption component fixed to the Galactic value $3.9 \times 10^{20} \text{ cm}^{-2}$, a pure neutral reflection component (`PEXRAV`) with a spectral index fixed to 1.8 and a gaussian Fe-K line. We used both `XSPEC` (ver. 12.7.1) and `SHERPA`³ with identical results. The extracted spectra and the best-fit parameters are presented in Figure 3 and Table 1⁴, respectively.

Given the contamination of the continuum emission by non-nuclear sources, our estimate of the nuclear continuum luminosity is an upper limit, and the Fe- K EWs must be considered as lower limits. The spectral analysis detects Fe-K line features in both regions, with comparable EW (1.1 keV and 0.9 keV in W and E region, respectively). As expected from the imaging, the Fe-K line is more luminous in the W nucleus ($5.7 \times 10^{39} \text{ erg s}^{-1}$) with respect to the E ($1.9 \times 10^{39} \text{ erg s}^{-1}$); we note that these values are consistent within errors with the narrow-band (6-7 keV) luminosities obtained with `APRATES` tool. As already discussed, the *observed* 2-10 keV luminosities, $3.2 \times 10^{40} \text{ erg s}^{-1}$ (W) and $1.3 \times 10^{40} \text{ erg s}^{-1}$ (E), should be considered as upper limits because of contamination.

Our detection of large Fe-K EWs from both nuclei may seem at odds with the results of LaMassa et al. (2011), who did not detect Fe-K emission using the same *Chandra* ACIS data. To investigate this discrepancy, we repeated the analysis of the entire central emission of Arp 220, following the procedure of these authors. Using a circular 4.5'' radius count extraction region centered at RA=15:34:57.194 DEC=+23:30:12.40, and their fitting model, we confirm their results (Table 2, left column of results). However, the authors fixed the Fe-K line rest-frame energy fixed at 6.4 keV. If, instead, we allow the gaussian line rest-frame energy to vary, we detect a line at $6.61 \pm 0.04 \text{ keV}$ with an equivalent width of $0.73^{+0.60}_{-0.30} \text{ keV}$, compatible with the *XMM-Newton* detection at $6.72 \pm 0.5 \text{ keV}$ (Iwasawa et al. 2005); all the other model parameters remain unchanged (see the right column in Table 2).

As demonstrated by Figures 1 and 2 there is no 6-7 keV emissions in regions outside the nuclei, even when the overall X-ray emission is more prominent. We have also extracted the spectrum of the softer luminous regions west of the W nucleus shown in Figure 2 (middle-right panel) centered at RA=15:34:57.207 DEC=+23:30:11.84, and find no evidence of line emission.

³<http://cxc.harvard.edu/sherpa>

⁴In the following, errors correspond to the 1- σ confidence level for one parameter of interest.

We analyzed the four archival *XMM-Newton* observations of Arp 220 (the two discussed in [Iwasawa et al. 2005](#), and two new ones performed in 2005) in order to test the possible contribution of a neutral iron emission line to the 6-7 keV emission we see in Figure 2. The data were reduced following a standard procedure, analogous to the one described by [Iwasawa et al. \(2005\)](#). The results are also in agreement: in a continuum plus single line model we obtain a best fit peak energy $E = 6.65 \pm 0.04$ keV. However, if we fit the data with two lines with fixed peak energies $E_1 = 6.4$ keV and $E_2 = 6.7$ keV, we obtain the results shown in Figure 4: a neutral component accounting for up to 40% of the observed line flux cannot be ruled out at a 90% confidence level.

If we then consider that 40% of the Fe-K line flux we estimate from *Chandra* spectra is due to Fe-K α neutral 6.4 keV emission line, the 2-10 keV *emitted* luminosities inferred from the Fe-K luminosities are 1.0×10^{42} erg s⁻¹ (W) and 0.4×10^{42} erg s⁻¹ (E). We note that these corrections are calibrated on “standard” obscured Seyfert galaxies, with an X-ray reflection efficiency of a few percent ([Levenson et al. 2006](#)). Hard X-ray observation of ULIRGs have demonstrated that on average this efficiency is much lower for these sources ([Nardini & Risaliti 2011](#); [Teng, Veilleux, & Baker 2012](#)). Consequently, the intrinsic X-ray luminosity of the two AGN detected here could be significantly higher. Considering the values for a standard reflection efficiency, the inferred X-ray luminosity is at least a factor of 3 higher than that expected from a pure starburst with the bolometric luminosity of Arp 220 ([Ranalli, Comastri, & Setti 2003](#)).

3. Discussion

The *Chandra* ACIS sub-pixel narrow-band imaging of the central region of the ULIRG merger Arp 220 provides compelling evidence of two CT AGNs, in both nuclei of the merging galaxies. Within the central 5''x5'', there are *only* two sources detected in the 6-7 keV band, containing the Fe-K lines. Although the E nucleus is detected with only 3 counts, the very low field background (~ 0.01) makes this a 5σ detection (Section 2). The centroids of these sources, $\sim 1''$ apart, are consistent, within *Chandra* astrometric uncertainty of 0.6'', with the position of the two NIR nuclear clusters identified by [Scoville et al. \(1998\)](#), and each coincident with a 6 cm VLA radio source ([Baan & Haschick 1995](#)) (Figure 1). We note that the W source is also consistent with the variable radio sources reported by [Batejat et al. \(2012\)](#). We stress that *no emission* in the 6-7 keV band is detected from other parts of the central region of Arp 220, even where the diffuse emission from the starburst is most intense. While the detections are highly significant for both nuclei, the fluxes are more uncertain, given the small number of detected photons (see Section 2).

The spectral analysis of both the central 4.5'' region, and of the individual E and W nuclei, results in the detection of emission lines. The rest energy of the line is larger than the 6.4 keV of the K α line, and suggests a contribution from 6.7 keV shock-ionized Fe xxv line as concluded

by Iwasawa et al. (2005), which could be associated with the starburst-induced shock (see e.g. the strong extended Fe xxv emission in NGC 6240 Wang et al. 2013). However, if we *assume* that both 6.4 keV and 6.7 keV lines are present in the spectrum, we obtain an acceptable fit to the *XMM-Newton* data which allow for 40% 6.4 keV contribution. The statistics, however, do not allow us to disentangle these two contributions to the observed emission in *Chandra* data. However, as discussed in Section 2, the line emission is only connected with the nuclear region, not with the more extended starburst. Although the uncertainties are large, we find large ~ 1 keV equivalent widths for the Fe-K lines; simulated data show that shock-ionized gas can yield comparable EWs for these lines, but would also yield continuum contribution much higher than we observe.

Besides a definite detection of hard photons (> 7 keV) from the W nucleus, which is also consistent with it being a CT AGN, the continuum emission from the nuclear regions is not easy to establish because of contamination from the surrounding emission in the 3-6 keV band. In particular, the W nucleus is significantly contaminated by the softer emission of a source or extended emission area nearby, which could be connected with the starburst phenomenon. This complex circumnuclear emission impedes the measurement of the nuclear continuum by means of spectral fitting. Any determination of the nuclear continuum with lesser spatial resolution data will give an even higher overestimation of its strength. Considering the above caveats, we can only set an upper limit of $< 2\%$ to the ratio between the observed and the inferred intrinsic luminosities for the two nuclear sources (see Section 2). This limit is consistent with the ratio between the observed luminosities of less obscured and CT AGNs (Maiolino et al. 1998). The spectra of the two nuclear sources presented in Figure 3 are in fact typical of CT AGNs, with observed Fe-K EW $\gtrsim 1$ keV.

The possibility of Arp 220 harboring one heavily obscured AGN has been discussed by Iwasawa et al. (2001, 2005) with *BeppoSAX* and *XMM-Newton* data; these authors conclude that, due to lack of hard emission above 10 keV, the CT AGN should be enshrouded in absorbing clouds with column density exceeding 10^{25} cm^{-2} and covering factor close to unity. Even ignoring the contamination of the continuum by extra-nuclear sources, the low counts in the two regions do not allow us to estimate absorption through spectral fitting. We can however compare the X-ray spectral energy distribution (SED) of the W source, for which we detect the hard nuclear continuum, with simulated spectra of obscured AGNs from Gilli, Comastri, & Hasinger (2007) (see Figure 5). For this purpose we use only the spectrum at energies > 5 keV, where the continuum is low and less contaminated by the nearby source (see Figure 3). The SED of the W nucleus is consistent with emission absorbed by $N_H \sim 10^{24.5} \text{ cm}^{-2}$. For comparison we extracted the spectrum from the bright region visible in Figure 2 (middle-right panel) west of W region; besides not showing any appreciable Fe-K feature, it is also compatible with absorbing column densities $< 10^{22} \text{ cm}^{-2}$.

The two nuclei have radio fluxes of 112 (W) and 88.2 (E) mJy (Baan & Haschick 1995), and X-ray to optical ratios $\alpha(ox) \approx 2.75$. From the inferred 2-10 keV emitted luminosities of the

two nuclear sources we evaluate bolometric luminosities assuming typical AGN SEDs (Elvis et al. 1994; Elvis, Risaliti, & Zamorani 2002), and the X-ray reflection efficiency of Seyfert galaxies, as discussed in Section 2. The estimated AGN bolometric luminosities, which should be regarded as lower limits, are $\sim 5.2 \times 10^{43} \text{ erg s}^{-1}$ (W) and $\sim 2 \times 10^{42} \text{ erg s}^{-1}$ (E). These represent only a few percent of Arp 220 bolometric luminosity, confirming that overall the emission of Arp 220 is dominated by the starburst component. This result is in broad agreement with the estimates from the mid-IR spectroscopy (Veilleux et al. 2009; Nardini et al. 2010). Lower limits on associated BH masses can be evaluated assuming Eddington limited accretion (with a standard 10% accretion rate to luminosity conversion efficiency), yielding $M \sim 3 \times 10^5 M_{\odot}$ (W) and $\sim 1 \times 10^5 M_{\odot}$ (E).

Our results add to the evidence of CT AGNs arising as a result of the later stages of the merging evolution in galaxies, which may trigger accretion onto the supermassive black holes (e.g., Van Wassenhove et al. 2012). After NGC 6240 (Komossa et al. 2003) and NGC 3393 (Fabbiano et al. 2011), Arp 220 provides the third clear case of the occurrence of this phenomenon in the near universe. As NGC 6240 (Komossa et al. 2003), Arp 220 is a highly disturbed system of galaxies engaged in a major merging interaction. The physical projected separation of the CT nuclei is $\sim 670 \text{ pc}$ in NGC 6240 and $\sim 370 \text{ pc}$ in Arp 220, suggesting that the latter may be in a more advanced stage of merging. The third case, the apparently regular early- type spiral NGC 3393, with two CT nuclei separated by 150 pc (Fabbiano et al. 2011), suggested instead a more evolved merger, or perhaps a minor merger of unequal size galaxies. Interestingly, following the discovery of the double nuclear X-ray source, evidence of a merger past has surfaced in the optical spectra of this galaxy (Contini 2012).

4. Conclusions

We have found compelling evidence for two CT AGNs, associated with the nuclei of the merging galaxies in the nearest ULIRG Arp 220, making this galaxy the third case of detection of close pair CT AGNs (a few 100 pc apart), after NGC 6240 and NGC 3393. These nuclei are the sole regions of significant 6-7 keV emission in the central 2 kpc of Arp 220. The data are consistent with Fe-K line emission although at an energy possibly higher than 6.4 keV of the Fe-K α line, suggesting substantial contribution from Fe xxv emission lines (see also Iwasawa et al. 2005). Our analysis of the entire *XMM-Newton* dataset confirms the presence of Fe xxv emission line, but allows 40% of the narrow-band emitted flux from the neutral 6.4 keV line. Albeit uncertain - the spectral analysis of these regions suggests large $\sim 1 \text{ keV}$ EWs. The W nucleus was also detected at hard ($> 7 \text{ keV}$) energies implying absorption $N_H \sim 10^{24.5} \text{ cm}^{-2}$; at such energies no continuum emission was detected from the E nucleus. Our results are consistent with previous multi-wavelength indications of nuclear activity in Arp 220 (see Section 1), and strengthen

the evolutionary association of merging and nuclear activity in galaxies (e.g., [Hopkins, McClure-Griffiths, & Gaensler 2008](#); [Van Wassenhove et al. 2012](#)). Based on the Fe-K detections, we infer lower limits on the bolometric luminosity of the AGNs of $5.2 \times 10^{43} \text{ erg s}^{-1}$ for the W AGN, and $\sim 2 \times 10^{42} \text{ erg s}^{-1}$ for the E AGN. These are a few percent of the total ULIRG bolometric luminosity, confirming that overall the emission of this source is dominated by the starburst component, as estimated from the mid-IR spectroscopy ([Veilleux et al. 2009](#); [Nardini et al. 2010](#)).

These results have only been possible because of the unmatched *Chandra* spatial resolution, and the use of sub-pixel imaging in narrow spectral bands, which expose the telltale Fe-K emission of CT AGNs, and give us a clear picture of the nuclear surroundings. Although the Fe-K band detections of the two nuclei are highly significant, the paucity of photons results in large uncertainties for all derived quantities. A significantly longer *Chandra*/ACIS exposure will be needed to firmly measure the emission parameters of the two nuclei.

We acknowledge useful comments and suggestions by our anonymous referee. We thank Jonathan McDowell for data analysis suggestions. This work is supported by NASA grant GO1-12125A. We acknowledge support from the CXC, which is operated by the Smithsonian Astrophysical Observatory (SAO) for and on behalf of NASA under Contract NAS8-03060. This research has made use of data obtained from the Chandra Data Archive, and software provided by the CXC in the application packages CIAO and Sherpa. This research has made use of Iris software provided by the US Virtual Astronomical Observatory, which is sponsored by the National Science Foundation and the National Aeronautics and Space Administration.

REFERENCES

- Aalto S., Wilner D., Spaans M., Wiedner M. C., Sakamoto K., Black J. H., Caldas M., 2009, *A&A*, 493, 481
- Baan W. A., Haschick A. D., 1995, *ApJ*, 454, 745
- Batejat F., Conway J. E., Rushton A., Parra R., Diamond P. J., Lonsdale C. J., Lonsdale C. J., 2012, *A&A*, 542, L24
- Clements D. L., McDowell J. C., Shaked S., Baker A. C., Borne K., Colina L., Lamb S. A., Mundell C., 2002, *ApJ*, 581, 974
- Contini M., 2012, *MNRAS*, 247
- Di Matteo T., Springel V., Hernquist L., 2005, *Natur*, 433, 604

- Downes D., Eckart A., 2007, *A&A*, 468, L57
- Elvis M., et al., 1994, *ApJS*, 95, 1
- Elvis M., Risaliti G., Zamorani G., 2002, *ApJ*, 565, L75
- Fabbiano G., Wang J., Elvis M., Risaliti G., 2011, *Natur*, 477, 431
- Fruscione, A., McDowell, J. C., Allen, G. E., et al. 2006, *Proc. SPIE*, 6270
- Gilli R., Comastri A., Hasinger G., 2007, *A&A*, 463, 79
- Harris, D. E., Mossman, A. E., & Walker, R. C. 2004, *ApJ*, 615, 161
- Hopkins A. M., McClure-Griffiths N. M., Gaensler B. M., 2008, *ApJ*, 682, L13
- Iwasawa K., Matt G., Guainazzi M., Fabian A. C., 2001, *MNRAS*, 326, 894
- Iwasawa K., Sanders D. B., Evans A. S., Trentham N., Miniutti G., Spoon H. W. W., 2005, *MNRAS*, 357, 565
- Kim D.-C., Sanders D. B., 1998, *ApJS*, 119, 41
- Komatsu, E., Smith, K. M., Dunkley, J., et al. 2011, *ApJS*, 192, 18
- Komossa S., Burwitz V., Hasinger G., Predehl P., Kaastra J. S., Ikebe Y., 2003, *ApJ*, 582, L15
- LaMassa S. M., Heckman T. M., Ptak A., Martins L., Wild V., Sonnentrucker P., Hornschemeier A., 2011, *ApJ*, 729, 52
- Levenson N. A., Heckman T. M., Krolik J. H., Weaver K. A., Życki P. T., 2006, *ApJ*, 648, 111
- Li, J., Kastner, J. H., Prigozhin, G. Y., & Schulz, N. S. 2003, *ApJ*, 590, 586
- Magorrian J., et al., 1998, *AJ*, 115, 2285
- Maiolino R., Salvati M., Bassani L., Dadina M., della Ceca R., Matt G., Risaliti G., Zamorani G., 1998, *A&A*, 338, 781
- Matt G., et al., 1997, *A&A*, 325, L13
- Matt G., Fabian A. C., Guainazzi M., Iwasawa K., Bassani L., Malaguti G., 2000, *MNRAS*, 318, 173
- Nardini E., Risaliti G., Watabe Y., Salvati M., Sani E., 2010, *MNRAS*, 405, 2505

- Nardini E., Risaliti G., 2011, MNRAS, 415, 619
- Paggi A., Wang J., Fabbiano G., Elvis M., Karovska M., 2012, ApJ, 756, 39
- Palmeri P., Mendoza C., Kallman T. R., Bautista M. A., Meléndez M., 2003, A&A, 410, 359
- Perlman, E. S., Padgett, C. A., Georganopoulos, M., et al. 2010, ApJ, 708, 171
- Ranalli P., Comastri A., Setti G., 2003, A&A, 399, 39
- Rangwala, N., Maloney, P. R., Glenn, J., et al. 2011, ApJ, 743, 94
- Risaliti G., Maiolino R., Salvati M., 1999, ApJ, 522, 157
- Sanders D. B., Mirabel I. F., 1996, ARA&A, 34, 749
- Scoville N. Z., et al., 1998, ApJ, 492, L107
- Siemiginowska, A., Stawarz, Ł., Cheung, C. C., et al. 2007, ApJ, 657, 145
- Soifer B. T., Sanders D. B., Madore B. F., Neugebauer G., Danielson G. E., Elias J. H., Lonsdale C. J., Rice W. L., 1987, ApJ, 320, 238
- Teng S. H., Veilleux S., Baker A. J., 2012, AAS, 220, #409.03
- Van Wassenhove S., Volonteri M., Mayer L., Dotti M., Bellovary J., Callegari S., 2012, ApJ, 748, L7
- Veilleux S., et al., 2009, ApJS, 182, 628
- Wang J., et al., 2011a, ApJ, 729, 75
- Wang J., Fabbiano G., Elvis M., Risaliti G., Mundell C. G., Karovska M., Zezas A., 2011b, ApJ, 736, 62
- Wang J., et al., 2011c, ApJ, 742, 23
- Wang J., et al., 2013, in preparation

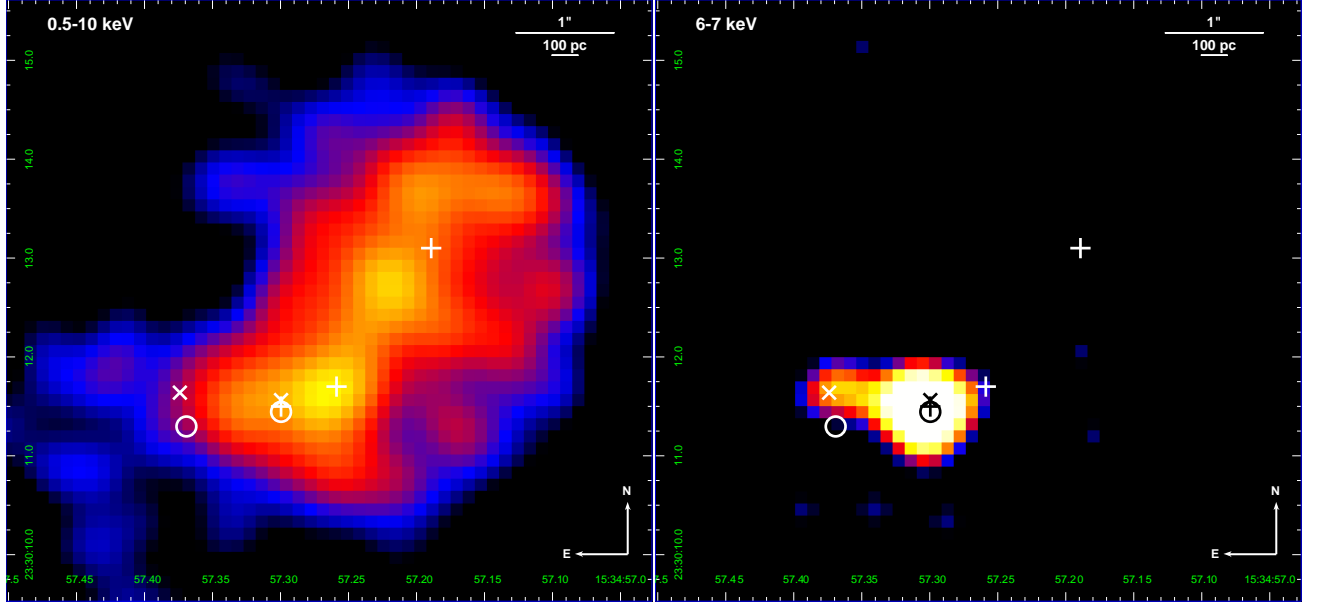


Fig. 1.— (Left frame) Full-band (0.5 – 10 keV) ACIS image with sub-pixel binning (1/4 of the native pixel size) and 2X2 FWHM gaussian filter smoothing; pluses (+) represent the *Chandra* hard X-ray sources reported by Clements et al. (2002), crosses (x) represent NICMOS near- infrared sources reported by Scoville et al. (1998), and circles (o) represent radio VLA 6 cm peaks reported by Baan & Haschick (1995), respectively. The colors of the symbols are chosen for visibility. (Right frame) Same of left frame but in the narrow 6 – 7 keV band.

Table 1: Spectral fitting for the iron regions

	W region	E region
Band	Net counts (error)	
3-8 keV	30(5)	7(3)
6-7 keV	12(3)	3(2)
Model parameter	Best-fit value	
E_{Fe-K} (keV)	$6.65^{+0.06}_{-0.05}$	$6.56^{+0.11}_{-0.10}$
$F_{Fe-K}(10^{-6} \text{ cm}^{-2} \text{ s}^{-1})$	$0.75^{+0.50}_{-0.37}$	$0.25^{+0.31}_{-0.19}$
$L_{Fe-K}(10^{39} \text{ erg s}^{-1})$	$5.70^{+3.77}_{-2.79}$	$1.87^{+2.32}_{-1.46}$
EW (keV)	$1.10^{+0.62}_{-0.75}$	$0.90^{+0.85}_{-0.79}$
C-stat (d.o.f.)	211.10(676)	
$L_{2-10 \text{ keV}}(10^{40} \text{ erg s}^{-1})$	$3.17^{+0.65}_{-0.67}$	$1.26^{+0.30}_{-0.36}$

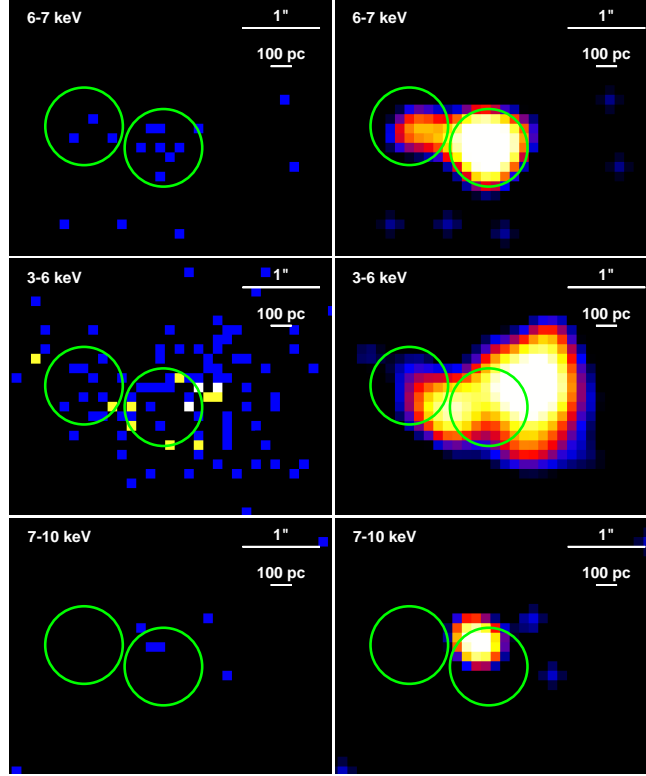


Fig. 2.— (Upper panel) Left frame: narrow band (6-7 keV) ACIS image with sub-pixel binning (1/4 of the native pixel size). In the color scale is blue corresponds to 1 count, yellow to 2 counts, and white to > 2 counts. The large circles are our count extraction areas. Right frame: same as left frame but with a 2X2 pixel FWHM gaussian filter smoothing applied. (Middle panel) Same as upper panel but in the 3-6 keV band. (Lower panel) Same as upper panel but in the 7-10 keV band.

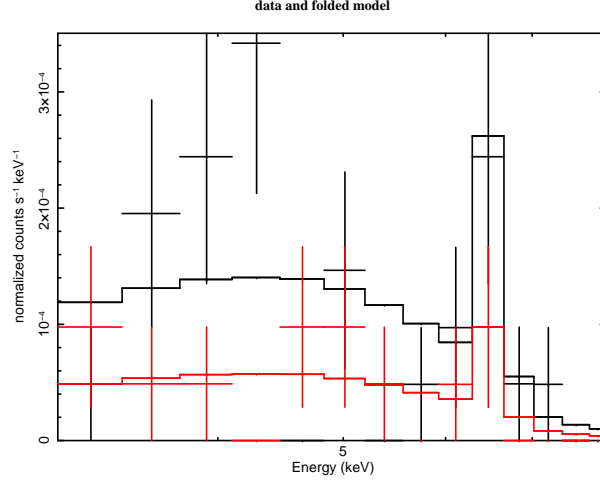


Fig. 3.— Best fit to spectra extracted from regions shown in Figure 2. The spectrum from W region is shown in black and the E region in red.

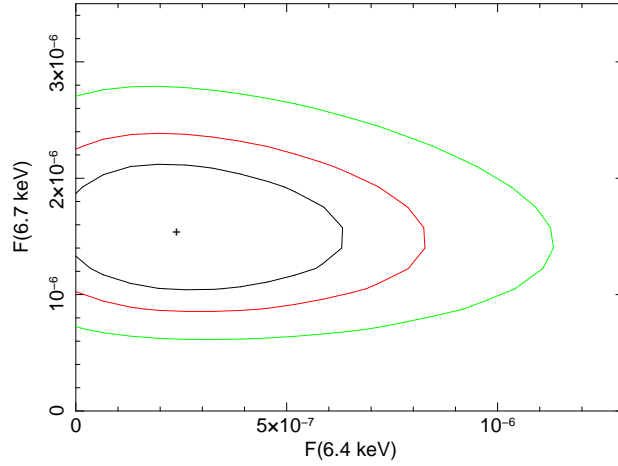


Fig. 4.— Contour plot for the relative flux of the 6.4 and 6.7 keV lines in a fit where both energies are fixed. The contours represent a probability of 68%, 90% and 99%. Even if a solution with a single 6.7 keV line is possible, a contribution of up to 40% by a neutral line is compatible with the data at a 90% confidence level.

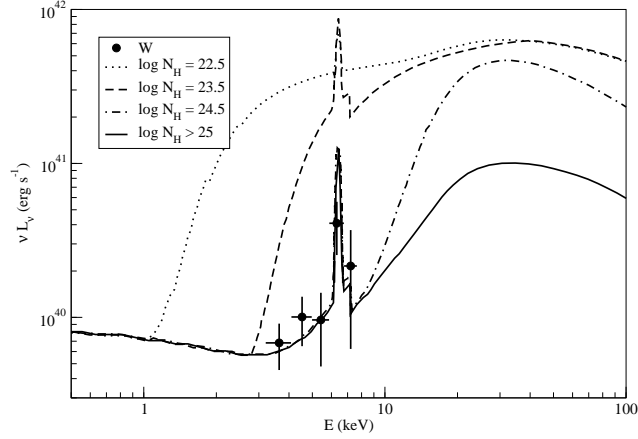


Fig. 5.— Rest frame SEDs of the W nuclear source in Arp 220 (black circles) compared with simulated AGN X-ray spectra with different absorbing column densities (Gilli, Comastri, & Hasinger 2007).

Table 2: Spectral fitting for the central 4.5'' region

Band	Net counts (error)	
0.5-10 keV	565(24)	
6-7 keV	17(4)	
Model parameter	Best-fit value	
N_H (cm ⁻²)	$0.76^{+0.14}_{-0.22}$	$0.73^{+0.15}_{-0.22}$
kT (keV)	$0.91^{+0.07}_{-0.06}$	$0.91^{+0.07}_{-0.06}$
Γ	$0.95^{+0.24}_{-0.28}$	$1.05^{+0.22}_{-0.27}$
E_{Fe-K} (keV)	6.4*	6.61 ± 0.04
F_{Fe-K} (10 ⁻⁶ cm ⁻² s ⁻¹)	< 0.32	$0.87^{+0.44}_{-0.36}$
L_{Fe-K} (10 ³⁹ erg s ⁻¹)	< 3.64	$6.61^{+3.34}_{-2.73}$
EW (keV)	< 0.42	$0.73^{+0.60}_{-0.30}$
C-stat (d.o.f.)	128.94(130)	123.42(129)
$L_{2-10 \text{ keV}}$ (10 ⁴⁰ erg s ⁻¹)	$7.80^{+0.66}_{-1.48}$	$7.89^{+0.43}_{-1.41}$